AIAA 82-4109

Theoretical Investigation of Sailwing Airfoils Taking Account of Elasticities

H. Murai* and S. Maruyama†
Tōhoku University, Sendai, Japan

In order to estimate sailwing performances theoretically, numerical analysis methods of the single and double membrane sailwings are presented, taking into consideration the elongation of the membrane and the elasticity of trailing-edge wire. Through the computational examples of the double membrane sailwings with various shape leading edges, it is shown that the decrease in the discontinuities of curvature at the points where the membranes separate from the leading-edge spar is effective for obtaining superior aerodynamic characteristics. The single membrane sailwing analysis demonstrates that the lift characteristics change by changing the trailing-edge parameters such as initial tension and elasticity of the trailing-edge wire. This is especially true for the latter, which mainly contributes to the nonlinear characteristics of the lift vs incidence relation. It is also shown that the lift vs incidence relations of double and single membrane sailwings are in good accordance if a leading-edge spar shape of a double membrane sailwing is symmetric on the upper and lower surfaces.

Nomenclature

c	= basic chord length
C_L	= lift coefficient
C_M	= moment coefficient
C_p	= pressure coefficient $= (P-P_\infty)/\frac{1}{2}\rho U_\infty^2$
C_{pi}	= internal pressure coefficient $= (P_i-P_\infty)/\frac{1}{2}\rho U_\infty^2$
C_T	= nondimensional tension $= T/\frac{1}{2}\rho U_\infty^2 c$
C_{T0}	= initial tension coefficient, Eq. (7)
K_t	= nondimensional spring constant of the trailing-edge wire
K_m	= nondimensional spring constant of the membrane per unit length
$\bar{K}_t$	= equivalent trailing-edge spring constant
l	= length of membrane between the leading edge (0,0) and the trailing edge (one side)
P, P_∞	= static pressure on wing surface, in freestream
P_i	= internal pressure of sailwing
t_i	= nondimensional length of the spring at unloaded position
T	= chordwise tension per unit span
T_0	= initial tension of the trailing-edge wire
U_∞	= freestream velocity
x,y,z	= Cartesian coordinates
α	= angle of attack
ΔC_p	= pressure difference coefficient $= (P-P_i)/(\frac{1}{2}\rho U_\infty^2)\{\tan^{-1}(\partial\eta/\partial\xi)\}$
ϵ	= nondimensional excess length of membrane $= (l/c)-1$
ϵ_0	= nondimensional excess length of membrane when unloaded
ξ, η	= nondimensional coordinates $= x/c, y/c$, respectively
ρ	= density
ϕ	= velocity potential

Subscripts

L	= leading-edge spar coordinate
m	= membrane coordinate
s	= separation point of leading-edge spar and membrane
t	= trailing edge
u, l	= upper surface, lower surface

Received March 16, 1981; revision received Sept. 24, 1981.

*Professor, Institute of High Speed Mechanics.
†Postgraduate Student, Department of Mechanical Engineering.

I. Introduction

THERE have been numerous experimental investigations performed on sailwings and their applications to the windmill generator because of their low cost and light structures. And at present, the aerodynamic performance of a sailwing with the so-called D-shape leading edge has become comparable to a rigid wing[1] by experimental trial and error processes.

In a previous report[2] a theoretical method for predicting the aerodynamic characteristics of a sailwing was presented. The difference between these characteristics and those of a rigid wing due to the deformation of sailwing surface was demonstrated numerically. In this report[2] it was assumed that the position of the trailing edge and the slacknesses of the wing surfaces were fixed. As is shown in Fig. 1, a sailwing

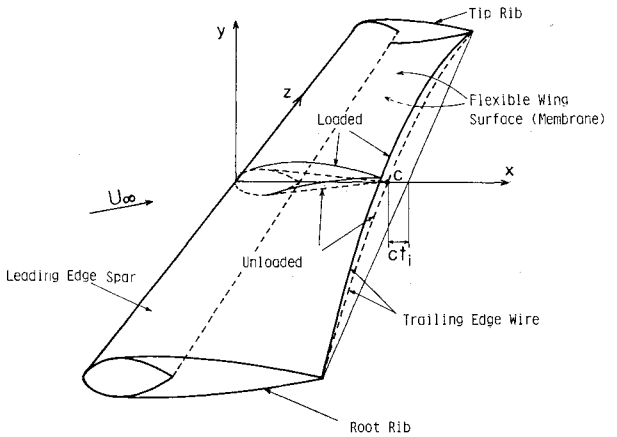

Fig. 1 Schematic figure of a sailwing structure.

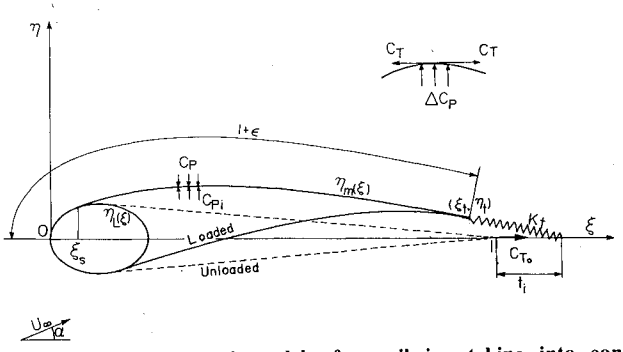

Fig. 2 Two-dimensional model of a sailwing taking into consideration the elasticity of the trailing-edge wire and membrane.

consists of a rigid leading-edge spar, a trailing-edge wire stretched between the tip and root ribs, and flexible wing surfaces which are wrapped around the leading-edge spar and the trailing-edge wire, forming the upper and lower surfaces. However, the trailing-edge moves and the wing surfaces elongate owing to the elasticities of trailing-edge wire and the wing surfaces when the sailwing is loaded.

In order to simulate the three-dimensional characteristics of the sailwing shown in Fig. 1, a simple, two-dimensional model of a sailwing airfoil at each streamwise cross section, as shown in Fig. 2, is adopted for the first stage of analysis. The present report will present a theoretical method of numerical analysis of the two-dimensional double and single membrane sailwing airfoils, taking into consideration the deflection of the trailing-edge wire and the elongation of the membrane due to the aerodynamic force. It is also going to show the effect of the initial tension on the sailwing membrane, and the elasticities of the trailing-edge wire and the membrane on the sailwing aerodynamic characteristics.

II. Basic Equations

When the sailwing is subjected to an aerodynamic load, the trailing-edge wire deflects and the upper and the lower surfaces are elongated owing to the increase of the tension on the membranes. This causes a deflection of the membrane and a decrease in the effective incidence because the trailing edge deflects in the direction of the membrane, as is shown in Fig. 2.

The coordinates of each surface are represented as follows:

$$\begin{aligned} \eta(\xi) &= \eta_L(\xi) \qquad 0 \le \xi \le \xi_s \\ &= \eta_m(\xi) \qquad \xi_s \le \xi \le \xi_t \end{aligned} \tag{1}$$

The relationship between the tension of the membrane and the difference between internal and external pressure is expressed as follows, considering that the membrane slope $(d\eta_m/d\xi)$ is small in practical sailwings:

$$C_T \frac{d^2\eta_m}{d\xi^2} = \mp \Delta C_p \tag{2}$$

where C_T is the nondimensionalized chordwise tension and ΔC_p is the nondimensionalized pressure difference in the direction perpendicular to the chord, and $(-)$ and $(+)$ indicate the upper and lower surfaces, respectively.

The boundary conditions of Eq. (2) are as follows: 1) the membrane separates smoothly from the leading-edge spar at the point ξ_s, and 2) ends at the trailing edge $\xi = \xi_t$.

$$\eta_m = \eta_L \quad \text{at} \quad \xi = \xi_s \tag{3}$$

$$\frac{d\eta_m}{d\xi} = \frac{d\eta_L}{d\xi} \quad \text{at} \quad \xi = \xi_s \tag{4}$$

$$\eta_m = \eta_t \quad \text{at} \quad \xi = \xi_t \tag{5}$$

The membrane lengths on the upper and lower surfaces are represented respectively as follows:

$$\int_0^{\xi_s} \sqrt{\{(d\eta_L)^2 + (d\xi)^2\}} + \int_{\xi_s}^{\xi_t} \sqrt{\left\{1 + \left(\frac{d\eta_m}{d\xi}\right)^2\right\}} d\xi = 1 + \epsilon \tag{6}$$

Equations (1-6) are satisfied independently for both the upper and lower surfaces.

In a practical sailwing, the deflection of the trailing edge changes at each streamwise cross section. For simplicity, the trailing-edge wire elasticity is approximated by the spring connected at the trailing edge and the point where the straight line between the root and tip ribs crosses the plane of streamwise cross section $(0,\ 1+t_i)$. The spring has a nondimensionalized spring constant K_t and is subjected to initial tension C_{T_0} when there is no aerodynamic force on the surfaces. The geometry of the trailing-edge wire and C_{T_0} have the following relationship:

$$C_{T_0} = \frac{d^2c(z)}{dz^2} \frac{T_0}{\frac{1}{2}\rho U_\infty^2 c} \tag{7}$$

The trailing edge is at (1, 0), and the slackness of the membrane on each side is ϵ_0 when there is no aerodynamic force.

The trailing-edge coordinates are defined where the tensions of the upper and lower surfaces and that of the spring are in balance. It is assumed that the slopes of the spring and that of membranes at the trailing edge are the same.

$$1 - \xi_t = \frac{C_{Tu} + C_{Tl} - C_{T_0}}{K_t} \tag{8}$$

$$\eta_t = (1 - \xi_t + t_i)\left(\frac{d\eta_{tu}}{d\xi} + \frac{d\eta_{tl}}{d\xi}\right)\Big/2 \tag{9}$$

It is also assumed that the membrane is subjected to half of the initial tension when there is no aerodynamic force on the airfoil.

The slackness of the membrane on each side is defined as

$$\epsilon = \epsilon_0 + \frac{(C_T - C_{T_0}/2)}{E_m} \tag{10}$$

where E_m is the spring constant of each membrane and is equal to $K_m/(1+\epsilon_0)$.

The resulting boundary value problem is to solve Eqs. (11), (12), and (13) under the boundary conditions represented by Eqs. (1-10).

$$\frac{\partial^2\phi}{\partial\xi^2} + \frac{\partial^2\phi}{\partial\eta^2} = 0 \tag{11}$$

$$\phi(\pm\infty, \pm\infty) = U_\infty(\xi\cos\alpha + \eta\sin\alpha) \tag{12}$$

$$\Delta C_p = \left[C_{pi} - 1 + \left(\frac{\partial\phi}{\partial\xi}\right)^2 + \left(\frac{\partial\phi}{\partial\eta}\right)^2\right]\cos\left\{\tan^{-1}\left(\frac{d\eta}{d\xi}\right)\right\} \tag{13}$$

III. Numerical Analysis

In order to solve the above boundary value problem, calculations of the effect of the pressure distribution on the sailwing surface deformation and the potential flow analysis around the deformed airfoil are carried out separately. The final solution is obtained in iterative fashion. A panel method is used for the calculation of the pressure distribution. In particular, a modification of the combination of Oellers' method[3] and that of Hess and Smith,[4] presented in a previous report,[2] is used. The calculation of the airfoil shape also involved an iteration process separating the calculations of the membrane shape and tension, and the calculations of the coordinates of the trailing edge and the membrane elongations. For the above iteration process, the so-called shooting method was used, which is described in the following section in order to obtain a fast convergence in the calculations.

IV. Calculation of Airfoil Deformation

When ΔC_p, ϵ, and the coordinates of the trailing edge are given, the coordinates of the membrane are obtained from Eq. (2) and the boundary conditions are expressed by Eqs. (3-5) as

$$\eta_m = \frac{1}{C_T}\int_{\xi_s}^{\xi}\int_{\xi_s}^{\xi} \mp \Delta C_p (d\xi)^2 + \frac{d\eta_{Ls}}{d\xi}(\xi - \xi_s) + \eta_{Ls} \tag{14}$$

$$C_T=\left\{\int_{\xi_s}^{\xi_t}\int_{\xi_s}^{\xi_t}\mp\Delta C_p(\mathrm{d}\xi)^2\right\}\Big/\left\{\eta_t-\eta_s-\frac{\mathrm{d}\eta_{Ls}}{\mathrm{d}\xi}(\xi_t-\xi_s)\right\} \quad (15)$$

Equation (6) is reduced in the case where the slope of the membrane is small:

$$\int_0^{\xi_s}\sqrt{\{(\mathrm{d}\eta_L)^2+(\mathrm{d}\xi)^2\}}+(\xi_t-\xi_s)\left\{1+\frac{1}{2}\left(\frac{\mathrm{d}\eta_{Ls}}{\mathrm{d}\xi}\right)^2\right\}+\frac{1}{2C_T^2}\int_{\xi_s}^{\xi_t}\left(\int_{\xi_s}^{\xi}\Delta C_p\mathrm{d}\xi\right)^2\mathrm{d}\xi+\frac{1}{C_T}\frac{\mathrm{d}\eta_{Ls}}{\mathrm{d}\xi}\times\int_{\xi_s}^{\xi_t}\int_{\xi_s}^{\xi_t}\mp\Delta C_p(\mathrm{d}\xi)^2=1+\epsilon \quad (16)$$

The solution of Eq. (16) is obtained in the following way. Calculate the left-hand side of Eq. (16) at a selected point on the leading-edge spar, and search for ξ_s satisfying the right-hand side of the equation. The coordinates of η_L and $\mathrm{d}\eta_L/\mathrm{d}\xi$ corresponding to ξ_s are obtained using Lagrange's interpolation. When the C_T and the coordinates of the membrane are obtained from the above calculation, the new approximation for the ϵ and trailing-edge coordinates are estimated from Eqs. (8-10). Hence the final airfoil coordinates are obtained in iterative fashion from Eqs. (14-16) and Eqs. (8-10), when the ΔC_p is given from the potential flow calculation.

In order to obtain a fast convergence in the iteration process, the so-called shooting method is adopted. This method evaluates the approximation for ϵ and the coordinates of the trailing edge. When ξ_t, ϵ_u, and ϵ_l change to $\xi_t+\mathrm{d}\xi_t$, $\epsilon_u+\mathrm{d}\epsilon_u$, and $\epsilon_l+\mathrm{d}\epsilon_l$, respectively, the tension on the membrane can be expressed as follows, provided the change in ξ_s is negligible:

$$C_{Tu}+\mathrm{d}C_{Tu}=C_{Tu}+\frac{\partial C_{Tu}}{\partial\xi_t}\mathrm{d}\xi_t+\frac{\partial C_{Tu}}{\partial\epsilon_u}\mathrm{d}\epsilon_u \quad (17)$$

$$C_{Tl}+\mathrm{d}C_{Tl}=C_{Tl}+\frac{\partial C_{Tl}}{\partial\xi_t}\mathrm{d}\xi_t+\frac{\partial C_{Tl}}{\partial\epsilon_l}\mathrm{d}\epsilon_l \quad (18)$$

The membrane tension C_T is calculated from Eq. (2) and boundary conditions Eqs. (3) and (5). If ξ_s and the integrated values are not changed by C_T, then the partial derivatives, $\partial C_T/\partial\xi_t$ and $\partial C_T/\partial\epsilon$ in Eqs. (17) and (18) are evaluated as follows:

$$\frac{\partial C_T}{\partial\epsilon}=-C_T^3\Big/\left[\int_{\xi_s}^{\xi_t}\left(\int_{\xi_s}^{\xi}\Delta C_p\mathrm{d}\xi\right)^2\mathrm{d}\xi-\left\{\int_{\xi_s}^{\xi_t}\int_{\xi_s}^{\xi_t}\mp\Delta C_p(\mathrm{d}\xi)^2\right\}^2\Big/(\xi_t-\xi_s)\right] \quad (19)$$

$$\frac{\partial C_T}{\partial\xi_t}=-\frac{\partial C_T}{\partial\epsilon}\left[1+\left\{\int_{\xi_s}^{\xi_t}\int_{\xi_s}^{\xi_t}\mp\Delta C_p(\mathrm{d}\xi)^2\right\}^2\Big/\{2(\xi_t-\xi_s)^2C_T^2\}-\frac{1}{2}\left(\frac{\eta_t}{\xi_t}-\frac{\eta_s}{\xi_s}\right)^2\right] \quad (20)$$

By substituting Eqs. (17) and (18) into Eqs. (8) and (10), three simultaneous equations are obtained as follows:

$$\begin{bmatrix}\frac{\partial C_{Tu}}{\partial\xi_t}+\frac{\partial C_{Tl}}{\partial\xi_t}+K_t, & \frac{\partial C_{Tu}}{\partial\epsilon_u}, & \frac{\partial C_{Tl}}{\partial\epsilon_l}\\ \frac{\partial C_{Tu}}{\partial\xi_t}, & \frac{\partial C_{Tu}}{\partial\epsilon_u}-E_{mu}, & 0\\ \frac{\partial C_T}{\partial\xi_t}, & 0, & \frac{\partial C_{Tl}}{\partial\epsilon_l}-E_{ml}\end{bmatrix}\begin{bmatrix}\mathrm{d}\xi_t\\ \mathrm{d}\epsilon_u\\ \mathrm{d}\epsilon_l\end{bmatrix}=\begin{bmatrix}(1-\xi_t)K_t-C_{Tu}-C_{T_l}+C_{T_0}\\ (\epsilon_u-\epsilon_{0_u})E_{mu}-C_{Tu}+C_{T_0}/2\\ (\epsilon_l-\epsilon_{0l})E_{ml}-C_{Tl}+C_{T_0}/2\end{bmatrix} \quad (21)$$

Upon solving these equations, the new approximations $\xi_t^*=\xi_t+\mathrm{d}\xi_t$, $\epsilon_u^*=\epsilon_u+\mathrm{d}\epsilon_u$, and $\epsilon_l^*=\epsilon_l+\mathrm{d}\epsilon_l$ are given. When the elongation of the membrane is neglected, the new approximation for the ξ coordinate of the trailing edge, ξ_t^*, is reduced to the following form by using the same process described above:

$$\xi^*=\xi_t+\mathrm{d}\xi_t=\xi_t+\frac{(1-\xi_t)\bar{K}_t-C_{Tu}-C_{Tl}+C_{T_0}}{\bar{K}_t+\partial C_{Tu}/\partial\xi_t+\partial C_{Tl}/\partial\xi_t} \quad (22)$$

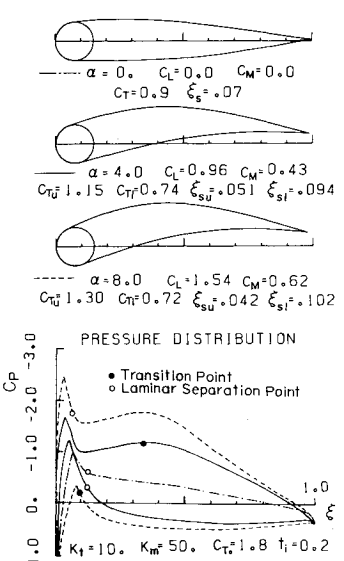

Fig. 3 Double membrane sailwing with round leading edge.

V. Calculation Results on Double Membrane Sailwings

The pressure distributions and profile forms for double membrane sailwings are shown in Figs. 3-5. These figures include values for the parameters, K_t, K_m, C_{T_0}, t_i, and α, as well as associated calculated values C_L, C_M, C_T, etc. Vaminar separation points predicted by the numerical method of Cebeci and Bradshaw,[5] and transition points predicted by Cebeci and Smith[6] at Reynolds number 2×10^6 are also shown in these figures. In these calculations, the first approximation for the pressure distribution is obtained by prescribing convex upper and lower surfaces and putting C_{pi} at zero.

The airfoil shapes with the round leading edge in Fig. 3 show that the camber becomes larger with increasing α. Consequently a larger C_L is obtained compared to a rigid airfoil at the same α. The pressure distributions in the figure have sharp peaks of minimum pressure coefficient near ξ_s and are apt to cause laminar boundary-layer separation on the leading edge spar. Similar pressure peaks were shown in a previous report.[2] Because the sailwing has the propensity to change airfoil shape, the pressure distribution on the lower surface is likely to cause laminar separation more easily than that on the upper surface at the small positive value of α. This C_p characteristic is considered to be one of the main reasons that the round leading-edge sailwing exhibits a rather poor performance at small incidence.[7]

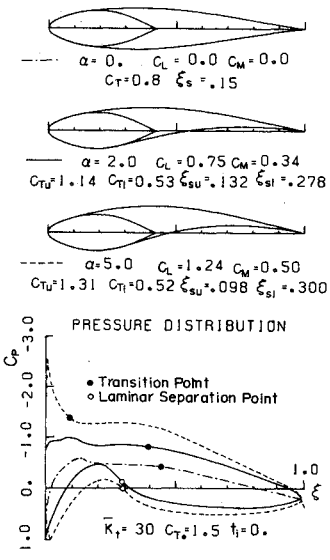

Fig. 4 Double membrane sailwing with symmetric D-shape leading edge reducing the discontinuities of curvature at ξ_s.

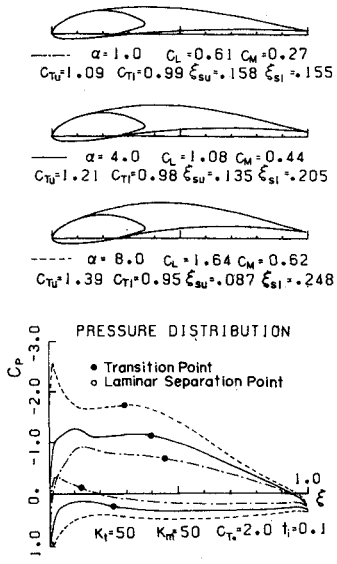

Fig. 5 Double membrane sailwing with unsymmetric D-shape leading edge.

One of the primary causes of the pressure peaks on the leading-edge spar is the strong discontinuity of curvature at the points where the membranes separate from the leading-edge spar. In order to reduce the discontinuities of curvature, the D-spar leading edge, which is symmetric with respect to the ξ axis, is used in Fig. 4. Within a 7% chord from the leading edge, the upper surface of the leading-edge spar has the same profile form as NACA 64(2)415 and connects to the rear part so smoothly that the curvature does not have strong discontinuities at ξ_s, taking into consideration the membrane tensions and ΔC_p. The elongation of the membrane is neglected in the calculation of Fig. 4. The relationship between the spring constants K_t and K_m and the reduced spring constant $\bar{K}_t$ neglecting K_m is approximated as follows, provided ϵ is small and K_m is not much smaller than K_t:

$$1/\bar{K}_t = 1/2K_m + 1/K_t \tag{23}$$

The pressure distributions in Fig. 4 show remarkable improvement in regard to the pressure peaks. But as the leading edge is symmetric, a region of relatively large velocity appears on the lower surface near the leading edge at $\alpha = 4$ deg, which reduces C_L compared to a conventional rigid airfoil with a relatively flat lower surface near a leading edge, and causes laminar separation when the Reynolds number is not large enough.

The sailwing in Fig. 5 has the unsymmetric D-shape leading edge having the same profile form as NACA 6412 within the 7.5% chord and connects to the rear part in the same manner as in Fig. 4. The large velocity regions on the lower surface near the leading edge in Fig. 4 are improved in the leading edge in Fig. 5. Hence this kind of unsymmetric D-shape leading edge is considered to be suitable for horizontal axis windmills or ultralight sailplanes, in which the expected range of incidence is mostly positive. Also the pressure distribution due to the large camber at $\alpha = 8$ deg seems to explain the experimental observation concerning D-shape leading edges by Sweeney,[8] which showed gentle turbulent boundary-layer separation from the trailing edge at a large incidence.

The airfoil profiles at $\alpha = 1$ and 4 deg in Fig. 5 are similar to that of NACA 4412 and 6412, respectively. NACA 4412 airfoil shows small drag at small lift but large drag at large lift, and the opposite is shown in NACA 6412.[9] This fact implies that a sailwing has small drag at small lift, and lift-drag and stall characteristics at large lift similar to a highly cambered rigid airfoil, provided the sailwing is properly designed with the aid of the theoretical investigations discussed above.

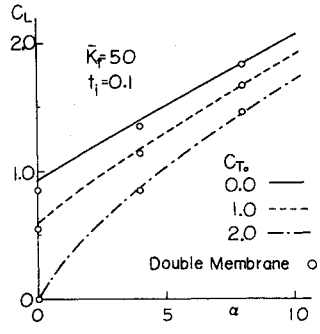

Fig. 6 Effect of initial tension on $C_L(\alpha)$ relations.

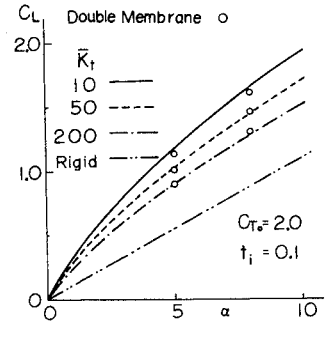

Fig. 7 Effect of spring constant of trailing-edge wire on $C_L(\alpha)$ relations.

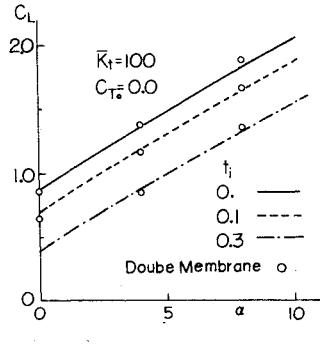

Fig. 8 Effect of parameter t_i on $C_L(\alpha)$ relations.

VI. Single Membrane Sailwings

In order to investigate the effect of the elasticity of the trailing-edge wire, the initial tension, and the parameter t_i, a numerical analysis of the single membrane sailwing is presented in this section.

The pressure difference ΔC_p in Eq. (2) becomes the pressure difference between the upper and lower surfaces, and the separation point goes to zero in the case of the single membrane. Then the relations for the single membrane sailwing can be used in the same manner as those for the double membrane. The same numerical calculation process shown in the previous sections is also adopted in the case of the single membrane,

$$C_T = C_{Tu} + C_{Tl} \tag{24}$$

$$\epsilon_0 = 0 \tag{25}$$

The relation between K_t, K_m, and $\bar{K}_t$ is as follows, provided that ϵ is small:

$$1/\bar{K}_t = 1/K_m + 1/K_t \tag{26}$$

This relationship is valid even if K_m is much smaller than K_t since there is no difference in ϵ on the upper and lower surfaces.

Figures 6-8 show $C_L(\alpha)$ relations for various combinations of the initial tension C_{T_0}, the elastic constant $\bar{K}_t$, and the length of the nondimensionalized spring t_i. The comparison between each single membrane sailwing and the double membrane sailwing with the round leading edge of 15% chord diameter at the same α and trailing-edge parameters: K_t, C_{T_0}, and t_i, is also shown in each figure. These comparisons show that the $C_L(\alpha)$ characteristics of the single membrane sailwing are almost the same as those of the double membrane sailwing if its leading-edge spar is symmetric with respect to the ξ axis and C_{pi} is zero. However the pressure distributions are different, as reported previously.[2] Hence the single membrane analysis is accurate enough for the estimation of total airfoil characteristics such as $C_L(\alpha)$.

Figure 6 shows that the $C_L(\alpha)$ characteristics change in both zero incidence lift and slope of the lift curves due to C_{T_0}, which suggests that the characteristics of sailwings can be changed widely by changing C_{T_0}.

Figure 7 shows the effect of the elastic constant of the trailing edge, $\bar{K}_t$. The lift slope is larger than that of the rigid wing shown by the double dotted line in Fig. 7, and is larger at a small α than at a large α, hence the $C_L(\alpha)$ relation becomes nonlinear. These characteristics were reported by Fink[10] Sweeney,[8] and Maughmer[1] in their wind-tunnel experiments. As $\bar{K}_t$ becomes smaller, the nonlinearity becomes larger because the change of the camber is larger in the sailwing with smaller $\bar{K}_t$.

It can be seen in Fig. 8, that as t_i increases, C_L decreases almost constantly because of the decrease in effective incidence due to the deflection of the trailing-edge wire. Among the effects of initial tension, spring constant and spring length on the $C_L(\alpha)$ relation, the last parameter is the most effective in decreasing the effective α, as expressed in Eqs. (8) and (9), which are related to C_T and the slope of the membrane at the trailing edge. These parameters are related to C_p and C_L. However, there is no explicit relation between the decrease in α and C_L at this stage.

VII. Conclusions

Theoretical methods have been developed for analyzing the characteristics and the profile form of double and single membrane sailwings, taking into consideration the elasticities of the trailing-edge wire and membranes, initial tension, and the length of the nondimensionalized spring. The main items demonstrated through the examples of the numerical analysis are as follows:

1) Comparing the pressure distributions with peaks which appeared on both surfaces of a double membrane sailwing with a round leading edge in a previous report,[2] it can be seen that the one on the lower surface can cause a laminar boundary-layer separation more easily than the other when incidence is small.

2) The profile form of the leading-edge spar, which eliminates the discontinuities of curvature at the separation point of the membrane from the leading-edge spar, weakens the pressure peaks. A drooped unsymmetric D-shape leading-edge spar is especially suitable for improving the pressure distribution on the lower surface, when the practical range of the incidence is expected to be positive.

3) The relationship of the lift vs the incidence of the single membrane sailwing is in good accordance with that of a double membrane sailwing.

4) The lift curve of a sailwing can be changed widely by changing the initial tension, spring constant, and the length of the spring, and is especially dominated by the initial tension.

5) The elasticity of the trailing-edge wire mainly affects the nonlinearity of the lift curve, as had been reported in experimental observations by a few authors.

6) A larger length of the spring decreases the effective incidence due to the movement of the trailing-edge wire in the direction of the membrane.

References

[1] Maughmer, M. D., "Optimization and Characteristics of a Sailwing Windmill Rotor," Princeton University, Princeton, N.J., AMS Rept. 1279, March 1976.

[2] Murai, H. and Maruyama, S., "Theoretical Investigation of the Aerodynamics of Double Membrane Sailwing Airfoil Sections," *Journal of Aircraft*, Vol. 17, May 1980, pp. 294-299.

[3] Ormsbee, A.I. and Chen, A.W., "Multiple Element Airfoils Optimized for Maximum Coefficient," *AIAA Journal*, Vol. 10, Dec. 1972, pp. 1620-1624.

[4] Hess, J.L. and Smith, A.M.O., *Progress in Aeronautical Sciences*, 1st ed., Vol. 8, Pergamon Press, New York, 1967, pp. 1-39.

[5] Cebeci, T. and Bradshaw, P., *Momentum Transfer in Boundary Layers*, 1st ed., McGraw Hill, New York, 1977.

[6] Cebeci, T. and Smith, A.M.O., *Analysis of Turbulent Boundary Layers*, Academic Press, New York, 1974.

[7] Buehring, I., "Performance Characteristics of Simple Airfoils for Windmill Applications," Department of Electrical Engineering Report, Imperial College, London University, Dec. 1977.

[8] Sweeney, T.E., "Exploratory Sailwing Research at Princeton," Princeton University, Princton, N.J., AMS Rept. 578, Dec. 1961.

[9] Jacobs, E.N., Ward, K.E., and Pinkerton, R.M., "The Characteristics of 78 Related Airfoil Sections from Test in the Variable-Density Wind Tunnel," NACA Rept. 460, 1933.

[10] Fink, M.P., "Full-Scale Investigation of the Aerodynamic Characteristics of a Model Employing a Sailwing Concept," NASA TN D-4062, July 1967.